Climate Dynamics (2002) 19: 155–166
DOI 10.1007/s00382-001-0219-3

M.T. Coe · S.P. Harrison

The water balance of northern Africa during the mid-Holocene: an evaluation of the 6 ka BP PMIP simulations

Received: 23 May 2001 / Accepted: 4 December 2001 / Published online: 28 February 2002

Abstract Runoff fields over northern Africa (10–25°N, 20°W–30°E) derived from 17 atmospheric general circulation models driven by identical 6 ka BP orbital forcing, sea surface temperatures, and CO_2 concentration have been analyzed using a hydrological routing scheme (HYDRA) to simulate changes in lake area. The AGCM-simulated runoff produced six-fold differences in simulated lake area between models, although even the largest simulated changes considerably underestimate the observed changes in lake area during the mid-Holocene. The inter-model differences in simulated lake area are largely due to differences in simulated runoff (the squared correlation coefficient, R^2, is 0.84). Most of these differences can be attributed to differences in the simulated precipitation ($R^2 = 0.83$). The higher correlation between runoff and simulated lake area ($R^2 = 0.92$) implies that simulated differences in evaporation have a contributory effect. When runoff is calculated using an offline land-surface scheme (BIOME3), the correlation between runoff and simulated lake area is ($R^2 = 0.94$). Finally, the spatial distribution of simulated precipitation can exert an important control on the overall response.

1 Introduction

Atmospheric general circulation models (AGCMs) represent the climate of the Earth through numerical solutions of the interactions of atmosphere, land, and ocean. The representation of the Earth's physical processes within AGCMs is somewhat simplified due to the uncertainties involved in the governing equations, the coarse spatial resolution of the models and limitations of available computational power. Despite the uncertainties these models are important tools for determining environmental and social policy (e.g. Kattenberg et al. 1996). For example, they are commonly used to determine likely changes in the climate at the land surface in response to anthropogenic changes in atmospheric composition and land use. However, the treatment of land-surface processes is necessarily simplified and as a result there is uncertainty about the reliability of model predictions. A clearer knowledge of the limitations and deficiencies in the models is therefore required.

The Project for Intercomparison of Land-Surface Parametrization Schemes (PILPS: www.gewex.com/pilps.html) was designed to understand the degree to which AGCM simulations of modern climate differ as a result of differences in the treatment of the land surface. Relatively few of the land-surface schemes examined in the first phase of the PILPS project were able to reproduce the observed patterns and magnitude of the components of the surface water budget (Shao et al. 1994). Offline investigations found large disparities in the surface energy balance between models (Pitman et al. 1993). Subsequent studies attributed these differences to the parametrizations describing energy fluxes at the land surface (Henderson-Sellers et al. 1995a, b; Henderson-Sellers 1996). However, the PILPS intercomparisons show that the accuracy of the simulation of surface water budgets is not correlated with model complexity (Desborough 1999).

Continued work within the PILPS project will doubtless produce a better understanding of and an improvement in land-surface schemes. However, while the accurate simulation of current climate is an important benchmark, it does not guarantee that a model can simulate climate changes correctly (Joussaume et al.

M.T. Coe (✉)
Center for Sustainability and the Global Environment,
Institute for Environmental Studies,
University of Madison-Wisconsin, 1225 W Dayton Street,
Madison, Wisconsin 53706, USA
E-mail: mtcoe@facstaff.wisc.edu

S.P. Harrison
Max Planck Institute for Biogeochemistry,
PO Box 100164, D-07701 Jena, Germany

1999). It is difficult to evaluate model performance solely on the basis of the instrumental record because the changes in climate since the middle of the last century have been relatively modest (e.g. Mann et al. 1995; Tett et al. 1999). Evaluating model performance under the extreme climate conditions experienced during the recent geological past provides an opportunity to evaluate how models respond to larger changes in forcing, and ultimately provides a key credibility test for modelling the future (Grassl 2000; Joussaume and Taylor 2000). The Paleoclimate Modelling Intercomparison Project (PMIP; Joussaume and Taylor 1995, 2000) has been engaged in such evaluations using rigorously standardized simulations for conditions representing last glacial maximum (LGM: 21,000 years before present, 21 ka BP) and middle Holocene (6000 years before present, 6 ka BP) climates and well-documented, palaeoenvironmental benchmark data sets (see e.g. Kohfeld and Harrison 2000; Harrison 2000).

Many of the evaluations of the PMIP simulations have focused on changes in the water budget of northern Africa as a consequence of the insolation-induced amplification of the Afro-Asian monsoon system at 6 ka BP. This focus has been motivated by the fact that the spatial expression of changes in the African monsoon system is comparatively simple, and that there are several well-documented data sets that show that the observed changes during the mid-Holocene were large. Comparisons with palaeoenvironmental data (e.g. Yu and Harrison 1996; Harrison et al. 1998; Joussaume et al. 1999) show that although the PMIP models all simulate a northward expansion of the monsoon front none produce an expansion as great as the observations would suggest. Joussaume et al. (1999) have quantified the mismatch between the simulated and observed climates, and demonstrated that the PMIP simulations underestimate the minimum amount of precipitation required to support the observed distribution of grassland and shrubland at about 23°N by between 50–100%. The range of the response of monsoon precipitation to orbital forcing shown by the models is large. Joussaume et al. (1999) suggest that, to some extent, the differences reflect differences in the simulated surface-energy balance.

In this study, we continue the investigations initiated by Joussaume et al. (1999) and present an analysis of the AGCM-simulated runoff fields in northern Africa at 6 ka BP. Runoff is a useful diagnostic because it integrates the precipitation and evaporation components of the hydrologic budget and is therefore sensitive to the treatment of the land surface within the AGCM. We use a hydrological routing algorithm (HYDRA; Coe 2000) to simulate the behaviour of the rivers, lakes, and wetlands in northern Africa in response to simulated changes in runoff at 6 ka BP. The simulated changes in runoff are derived in two ways: either directly from the PMIP simulations or indirectly, by using the changes in precipitation, temperature and cloudiness simulated by each of the PMIP simulations to drive an offline land-surface model. Comparisons of these two sets of simulations enable us to investigate the degree to which differences in the simulated runoff and lake area over northern Africa reflect differences in the land-surface schemes used by individual PMIP models and the distribution of simulated precipitation on the landscape.

2 Methods

2.1 The PMIP 6 ka BP simulation

The PMIP 6 ka BP simulation was conceived to examine the climate response to insolation forcing of different AGCMs (Joussaume and Taylor 1995, 2000). The 6 ka BP simulation therefore differs from the control simulation in only two respects: orbital parameters were changed and atmospheric CO_2 concentration was lowered to pre-industrial levels (Table 1; Joussaume et al. 1999). The lowering of CO_2 concentration is assumed to have only a minor effect on the

Table 1. Boundary conditions and general specifications of the PMIP control and 6 ka yr BP experiments

	Modern (control)	6000 years BP experiment	Source reference
Sea surface temperature	Existing control run or 10-year average of AMIP (1979–1988) data set	As modern	
Sea ice distribution	Existing control run or 10-year average of AMIP (1979–1988) data set	As modern	
Land–sea distribution and land topography	Existing control run	As modern	
Ice sheet distribution	Existing control run	As modern	
Land albedo	Existing control run	As modern	
CO_2	Existing control run or 345 ppmv	280/345 × control run level or 280 ppmv	Raynaud et al. 1993
Insolation			Berger 1978
Solar constant	Existing control run or 1365 W m–2	As modern	
Eccentricity	0.016724	0.018682	
Obliquity	23.446	24.105	
Perihelion (° from equinox)	102.04	0.87	
Definition of seasons	Existing control run	As modern	
Number of years simulated	11 (minimum)	11 (minimum)	
Length of ensemble	10	10	

simulated climate. Sea-surface temperatures (SSTs) and land-surface conditions, including the distribution of land and land ice, albedo and surface roughness, were prescribed to be the same in the 6 ka BP simulation as in the modern control simulations.

The 6 ka BP simulation has been performed by 18 different climate models within PMIP (Joussaume et al. 1999). One of these models (MSU: Moscow State University) has only been run at very low resolution (10 × 15 grid cells, with three levels in the vertical) and has therefore been omitted from our analyses. The remaining models are all full atmospheric general circulation models (AGCMs), but with very different parametrizations and a range of horizontal and vertical resolutions. A complete description of each of the models is given at the PMIP website (www-pcmdi.llnl.gov/pmip/). A summary of those aspects of the models and their land-surface schemes that are most pertinent to our analyses of the simulated hydrological cycle is given in Table 2.

3 Experimental design

Our evaluations of the PMIP simulations are confined to northern Africa (here defined as 10–25°N, 20°W–30°E). The expansion of the monsoon in response to orbital forcing during the early- to mid-Holocene is documented by the expansion of lakes and wetlands (e.g. Street and Grove 1976; Petit-Maire and Riser 1981, 1983; Gasse 1987; Pachur and Kröpelin 1987; Petit-Maire 1989; Arnold and Petit-Maire 1991; Pachur and Hoelzmann 1991; Street-Perrott and Perrott 1993) and by the existence of moisture-demanding vegetation (e.g. Maley 1981, 1983; Ritchie et al. 1985; Ritchie and Haynes 1987; Schulz 1991; Street-Perrott and Perrott 1993) in now-arid areas of northern Africa. Quality-controlled syntheses of these data are available (Qin et al. 1998; Jolly et al. 1998; Kohfeld and Harrison 2000; Harrison 2000), and earlier versions of these data sets have been used to evaluate palaeoclimate model simulations (e.g. Yu and Harrison 1996; Coe 1997; Pollard et al. 1998; Texier et al. 1997; Broström et al. 1998; Jolly et al. 1998; Vettoretti et al. 1998; Joussaume et al. 1999; Kutzbach et al. 2001). Our focus on northern Africa is partly motivated by the existence of these well-documented benchmark data sets. An additional motivation is provided by the fact that the structure of the African monsoon is relatively zonal (e.g. Rowell et al. 1995) and thus diagnosis of the simulated changes in the monsoon, and its impact on the hydrological balance of northern Africa, should be straightforward compared to the situation in other regions with monsoonal-type rainfall. The simulated climate of northern Africa has been a major focus of PMIP diagnoses, see e.g. Yu and Harrison (1996), Harrison et al. (1998), Joussaume et al. (1999) and Braconnot et al. (2000), Bonfils et al. 2001.

We ran two sets of simulations. In the first set, (referred to as **AGCM-run** in text), a hydrological routing model (HYDRA: Coe 1998, 2000) is forced with the 6 ka BP runoff, precipitation, and evaporation anomaly fields derived from the PMIP simulations. The results from AGCM-run investigate the impact of the change in the surface water balance simulated by each AGCM. Since the precipitation distribution and land-surface scheme of each AGCM strongly impact the resultant simulated runoff, we designed a second set of simulations (referred to as **BIOME-run** in the text) in which we derived runoff consistent with the climate anomalies simulated by each of the PMIP models offline using the land-surface scheme from a terrestrial biogeography model (BIOME3: Haxeltine and Prentice 1996). The runoff fields simulated by BIOME3 were then used as input to HYDRA to determine their effect on lake levels. Thus, the BIOME-run isolates the impact of the different AGCM land surface schemes by replacing them with a single land surface scheme. Analysis of the results of these two sets of simulations allows us to (a) quantify the simulated monsoon response to orbital forcing in terms of changes in lake area which can be directly compared to observations of lake area at 6 ka BP, (b) identify common features of the simulated hydrological changes, and (c) identify land-surface models which behave significantly different within the group of models.

3.1 The HYDRA model

HYDRA (the HYDrological Routing Algorithm) simulates the time-varying flow and storage of water in terrestrial hydrological systems, including rivers, wetlands, lakes, and human-made reservoirs (Coe 1998, 2000). The model derives river paths and potential lake and wetland volumes from digital elevation model (DEM) representations of the land surface. The model currently operates on the global scale at 5-min spatial resolution (~9 km at the equator). The physical land surface of HYDRA is coupled to a linear reservoir model to simulate (a) the discharge of river systems, and (b) the spatial distribution (and volume) of large lakes and wetland complexes. Rivers, lakes, and wetlands are defined as a continuous hydrologic network in which locally derived runoff is transported across the land surface in rivers, forms lakes and wetlands, and is eventually discharged into the ocean or evaporated from an inland water body. The model does not explicitly simulate groundwater discharge or drainage.

HYDRA is forced by surface runoff, plus precipitation and evaporation (in order to account for the water balance over lakes and wetlands themselves). Precipitation and surface runoff are derived from the PMIP AGCM simulations. The estimates of evaporation from surface waters are calculated at 0.5° resolution using the Penman formulation relating equilibrium evaporation from a wet surface to the net surface radiation (Peixóto and Oort 1992). Again, the temperature and cloudiness data required to calculate evaporation in this way are derived from the PMIP AGCM simulations. A complete description of HYDRA is provided by Coe (2000).

HYDRA successfully produces the modern observed global distribution of lakes and wetlands (Coe 1998) and has been extensively tested in northern Africa. The model has been shown to accurately simulate the monthly mean discharge and area of Lake Chad drainage basin for the 40-year period 1956–1995 (Coe and Foley 2001). HYDRA has also been used to evaluate the accuracy of AGCM simulated runoff for the modern climate (Coe 2000; Lenters et al. 2000).

For the AGCM-run simulations, we derived the runoff and precipitation forcing for HYDRA by interpolating the anomalies (difference between 6 ka and 0 ka BP simulations) of annual mean runoff and precipitation from the AGCM grid to the 5-minute horizontal resolution of HYDRA. These anomalies were then added to the annual mean runoff and annual mean precipitation estimates used for the modern (control) HYDRA simulation. Specifically, we used modern runoff estimates from Cogley (1989) and precipitation estimates from Legates and Willmott (1990a). The change (6 ka–0 ka) in simulated monthly average temperature and cloudiness are added to the observed surface temperature of Legates and Willmott (1990b) and potential sunshine (i.e. the inverse of observed cloudiness) from Leemans and Cramer (1991). These values are linearly interpolated to quasi-daily values and used to derive the net surface radiation. Annual mean evaporation was calculated by summing the daily equilibrium evaporation values.

3.2 The BIOME3 model

The coupled carbon- and water-flux module of the equilibrium terrestrial vegetation model BIOME3 (Haxeltine and Prentice 1996) was used to provide an independent offline estimate of runoff consistent with the precipitation, temperature and radiation budget simulated by each of the AGCMs (**BIOME-run**).

BIOME3 initially predicts the potential presence/absence of five woody and two non-woody plant functional types (PFTs) based on ecophysiological constraints. Differences in the physiology, phenology and rooting profile of these different PFTs affect their behaviour in the coupled carbon- and water-flux module. Competition between the PFTs is implicitly simulated as a function of relative net primary productivity (NPP). An optimisation algorithm is used to calculate the maximum sustainable leaf area (LAI) of each PFT and the associated NPP. Evapotranspiration (AET) is

Table 2. Characteristics of the land-surface schemes used by each of the 17 PMIP models used in this analysis

Code	Model name	Resolution	Soil hydrology	Soil treatment	Vegetation	Reference for land-surface schemes	References: to model and 6 ka BP simulation
BMRC	Bureau of Meteorology Research Centre Version 3.3	R21, L9	Single-layer bucket	1 soil type	No explicit vegetation	McAvaney and Hess (1996)	
CCC2	Canadian Centre for Climate Modelling and Analysis Version 2	T32 (96*48), L10	Single-layer bucket	1 soil type	24 soil/vegetation types	Wilson and Henderson-Sellers (1985)	McFarlane et al. (1992); Vettoretti et al. (1998)
CCM3	NCAR Community Climate Model, run at Center for Climatic Research, Madison Visconsin	T42 (128*64), L18	LSM	3 soil types (sand, silt, clay)	12 vegetation types	Bonan (1996)	Kiehl et al. (1996)
CCSR1	Center for Climate System Research	T21 (64*32), L20	Single-layer bucket	1 soil type	No explicit vegetation	Manabe (1965)	Numaguti et al. (submitted)
CNRM2	Centre National de Recherches Météorologiques Version 2	T31 (96*48), L19	ISBA (Noilhan and Planton 1989)	Specify albedo and % silt, sand, clay	13 vegetation types	Mahfouf et al. (1995) Manzi and Planton (1994)	
CSIRO	Commonwealth Scientific and Industrial Research Organisation Version 4.7	R21 (64*32), L20	SVAT	9 soil types	12 vegetation types	Kowalczyk et al. (1991, 1994)	
EC-HAM3	Max Planck Institute for Meteorologie, run at Bremen University Version 3.6	T42 (128*64), L19	Single-layer bucket	1 soil type	Forest, other vegetation, bare ground	Wilson and Henderson-Sellers (1985) Miller et al. (1992)	Lorenz et al. (1996)
GEN2	National Center for Atmospheric Research, GENESIS model, run at NCAR Version 2	T31 (96*48), L18	6-layer soil	1 soil type	EVE (Bergengren et al. 1997), predicts 110 life forms	Pollard and Thompson, (1995)	Pollard et al. (1998)
GFDL	Geophysical Fluid Dynamics Laboratory	R30 (96*80), L20	Single-layer bucket	No explicit variation	No explicit vegetation	Manabe et al. 1969	
GISS	Goddard Institute for Space Studies Version V.Iiprime	72*46, L9	6-layer soil	106 soil types	Vegetation type is a composite of 32 classifications	Rosenzweig and Abramopoulos (1997)	
LMD4	Laboratoire de Météorologie Dynamique, run at LSCE Version 4ter	48*36, L11	Single-layer bucket	1 soil type	No explicit vegetation	Manabe et al. (1969)	Sadourny and Laval (1984) Masson and Joussaume (1997)
LMD5	Laboratoire de Météorologie Dynamique, run at LSCE Version 5.3	64*50, L11	Sechiba	1 soil type	7 vegetation types and bare ground	Ducoudré et al. (1993)	Harzallah and Sadourny (1995) Masson and Joussaume (1997)
MRI2	Meteorological Research Institute Version Iib	72*46, L15	4-layer soil	1 soil type	No explicit vegetation	Noda et al. (1995)	Kitoh et al. (1995, 1998)
UGAMP	UK Universities Global Atmospheric Modelling Programme, run at Reading Version 2	T42 (128*64), L19	3-layer soil	1 soil type	No explicit vegetation	Dong and Valdes (1995)	Valdes and Hall (1994); Dong and Valdes (1995); Hall and Valdes (1997)
UIUC11	University of Illinois Urbana-Champagne	72*46, L11	Single-layer bucket	5 soil textures	7 vegetation types	Manabe et al. (1969)	
UKMO	UK Meteorological Office Unified Model, Version 3.2	96*73, L19	Single-layer bucket	3 soil types (coarse, medium, fine)	53 land cover types	Warrilow et al. (1986, 1989)	Hewitt and Mitchell (1997)
YONU	Yonsei University, Version Tr7.1.1	72*46, L8	Single-layer bucket	1 soil type	No explicit vegetation	Tokioka et al. (1984); Ghan et al. (1982)	

a function of equilibrium evapotranspiration rate (i.e. the evapotranspiration rate dependent on energy supply alone), potential (non-water limited) canopy conductance and soil moisture. A simple planetary boundary layer parametrization adapted from Monteith (1995) is used to relate non-water-limited potential canopy conductance and equilibrium evapotranspiration. When soil supply is limiting, canopy conductance and AET are reduced to match a supply-limited maximum transpiration rate. Minimum canopy conductance (which represents plant water loss not explicitly linked to photosynthesis) is a PFT-specific characteristic; potential maximum canopy conductance is implicitly so because optimum photosynthesis rates differ among PFTs. The soil water budget is calculated using a two-layer soil (0–50 mm, 50–150 mm). The maximum available water holding capacity of each layer is a texture-dependent parameter. The soil moisture content in each layer is calculated on a daily basis, as a function of precipitation, snowmelt, percolation between the soil layers, AET and runoff. The percolation rate is dependent on texture and the wetness of the upper soil layer. Runoff occurs from a given soil layer when that layer is saturated.

A full description and validation of the BIOME3 model is given in Haxeltine and Prentice (1996). The BIOME3 model successfully reproduces the distribution of potential natural vegetation (Haxeltine and Prentice 1996), and gives estimates of NPP and LAI that are in reasonable agreement with observations (Moore et al. 1995). The coupled carbon- and water-flux module used in BIOME3 successfully reproduced soil moisture and evaporation data used in the evaluation of land-surface models participating in PILPS (Shao et al. 1994). Indeed, the coupled carbon- and water-flux module was able to reproduce total growing season evapotranspiration more accurately than any other participating scheme, and was one of only 4 models that produced total annual runoff that fell within the range of the observations (Shao et al. 1994).

In the BIOME-run simulations, we interpolated the simulated anomalies (6 ka–0 ka) of mean monthly temperature, precipitation and cloudiness from the AGCM grid to the 0.5° resolution of BIOME3. The anomalies were added to a modern climatology (Cramer 2.2), which is an improved version of the Leemans and Cramer (1991) data set. Quasi-daily values of each of these variables were derived by linear interpolation between mid-month values. These climate data were then used to run BIOME3. The mean annual runoff fields simulated by BIOME3 were then used to force HYDRA (in addition to the same lake precipitation and evaporation used in **AGCM-run**).

4 Results

4.1 AGCM-run

The simulated modern area of lakes in northern Africa (10–25°N, 20°W–30°E) is about 63,000 km^2, which is roughly comparable with the estimated area of modern perennial lakes of 43,000 km^2 based on the Cogley (1989) data set. The lake area in northern Africa simulated using anomalies from the PMIP 6 ka BP simulations varies from about 30,000 km^2 to 163,000 km^2. Thus, the PMIP simulations produce changes in lake area of between 25,000 km^2 less to 100,000 km^2 greater than the simulated modern area (Fig. 1). The largest extent of surface water at 6 ka BP is simulated with runoff from the GENESIS2 and CNRM-2 models. Six of the simulations result in no significant increase in lake area or a decrease at 6 ka BP compared to modern (UIUC11, CSIRO, CCC2.0, YONU, CCSR1, CCM3). The smallest lake areas are simulated with runoff from

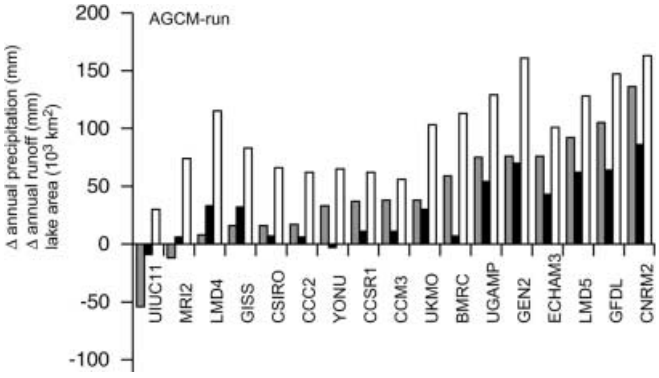

Fig. 1. Changes in annual precipitation (in mm) in *grey* and annual runoff (mm) in *black* simulated by the 17 PMIP models (6 ka BP–0 ka BP) compared to lake area (10^3 km^2) in *white* simulated in the HYDRA AGCM-run, all averaged over northern Africa (10–25°N, 20°W–30°E)

the UIUC11 (30,000 km^2) and CCM3 (56,000 km^2) models. Both of these models produce a total area of lakes *less* than 63,000 km^2 simulated under modern climate conditions.

The increased lake area simulated by most of the models is consistent with a northward expansion of the monsoon front in northern Africa and an increase in the annual mean precipitation. However, Hoelzmann et al. (1998) estimate that at least 5% (i.e. ca 570,000 km^2) of the land area of northern Africa was covered by perennial lakes at 6 ka BP. The largest simulated lake extent at 6 ka BP (163,000 km^2) is only 28% of the Hoelzmann et al. (1998) estimate.

Lake Chad, with an area of about 350,000 km^2 at 6 ka BP (Schneider 1967; Pias 1970), represents about 60% of the observed increase in water area at 6 ka BP (Hoelzmann et al. 1998). The average simulated area of Lake Chad of all 17 models is about 74,000 km^2, which is about 20% of the observed 6 ka BP area. Only four models (UGAMP, GENESIS2, GFDL, and CNRM-2) simulate a change in runoff large enough to produce a Lake Chad of greater than 100,000 km^2 and the largest is 135,000 km^2 (less than half of the observed 6 ka BP lake area). The smallest 6 ka BP Lake Chad (about 15,000 km^2) is from the UIUC11 runoff (about 10,000 km^2 less than the modern simulation). All models underestimate the area of Lake Chad in comparison to palaeo-observations. However, the underestimation is smaller than the underestimation of the total observed lake area in northern Africa. Twelve of the 17 models simulate more than 70% of the water area of northern Africa to be in the Lake Chad basin (Fig. 2). Three of these models (UKMO, UGAMP, and GFDL) result in greater than 80% of the simulated surface water being in Lake Chad. This suggests that many of the models simulate very low precipitation and runoff rates outside of the Chad basin.

There is considerable variation in the magnitude of the simulated precipitation change amongst the models

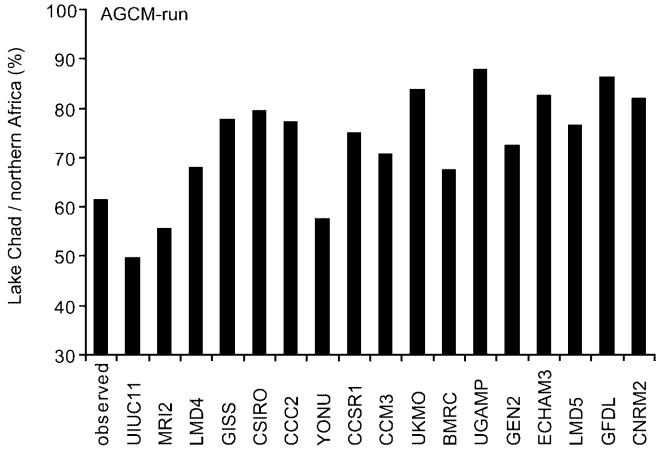

Fig. 2. The area of Lake Chad as a percentage of the total lake area for northern Africa (10–25°N, 20°W–30°E) for the observations of Cogley (1989) and the 17 PMIP models as simulated in the HYDRA AGCM-run

(Table 3, Fig. 1; see also Joussaume et al. 1999). Models with a higher simulated precipitation rate at 6 ka BP (relative to the other models) tend to simulate more runoff (Fig. 3a) and hence larger increases in lake area (Fig. 3b, 3c). However, the runoff and lake area do not increase identically with increased precipitation: models with nearly identical changes in precipitation produce simulated runoff that is very different. Indeed, there is as much as a two-fold difference between simulated lake areas for models with nearly identical simulated changes in precipitation (Fig. 1 and Table 3, compare results for CCSR1, CCM3 and UKMO or UGAMP, GENESIS2 and ECHAM3). In extreme cases, the simulated lake area is opposite to that expected from the precipitation change. In the case of MRI2, e.g. the runoff and lake area of northern Africa at 6 ka BP is greater than that of the modern simulation despite a decrease in the annual mean precipitation and, with CCM3, the lake area decreases slightly despite a large precipitation increase (Fig. 1, Table 3). These results imply that differences in simulated runoff are influenced by differences in how the AGCM land surface models redistribute incoming precipitation and energy into latent (evaporation) and sensible heat fluxes and the resultant surface temperature and evaporation and where the precipitation falls on the landscape.

4.2 BIOME-run

The lake area for northern Africa simulated by HYDRA using runoff from the BIOME3 land-surface scheme varies from 40,000 km^2 (UIUC11) to 270,000 km^2 (GFDL) (Fig. 4). Thus, the simulations produce changes in lake area of between 19,000 km^2 less than the simulated modern area to 211,000 km^2 greater than the simulated modern area. The range between the models appears to be enhanced compared to the AGCM-run. However, the average runoff for the 17 models simulated in BIOME3-run is about 30% greater than in AGCM-run (Table 3, Fig. 6). As a result, the average lake area simulated with BIOME3 runoff is about 44,000 km^2 larger than the simulation with the AGCM runoff directly (Figs. 3c, 5c). The difference in mean lake area between BIOME-run and AGCM-run indicates that (for a specific precipitation, temperature, and cloudiness) BIOME3 partitions less energy for evapotranspiration than most of the AGCMs (Fig. 6).

Figure 7 summarizes the difference in lake area simulated by each model for northern Africa in the AGCM-run compared to the BIOME-run. The average lake area simulated for the 17 models in AGCM-run varies from 30% greater (BMRC) to 65% smaller (CCM3) than the BIOME-run. When the difference is large and negative, then the AGCM-run had much smaller lake area than

Table 3. Summary of the simulated precipitation (P), runoff (R) in mm/year and runoff/precipitation ratio (R/P) derived from each of the 17 PMIP model simulations compared to the runoff and runoff/precipitation ratio derived for each simulation using the BIOME model

Model Code	AGCM-derived values			BIOME 3-derived values	
	P	**R**	**R/P**	**R**	**R/P**
BMRC	445	47	0,11	55	0,12
CCC2	403	46	0,11	84	0,21
CCM3	424	51	0,12	78	0,18
CCSR1	423	51	0,12	108	0,26
CNRM2	522	126	0,24	156	0,30
CSIRO	402	47	0,12	76	0,19
ECHAM3	462	83	0,18	102	0,22
GEN2	462	110	0,24	120	0,26
GFDL	491	104	0,21	151	0,31
GISS	402	72	0,18	65	0,16
LMD4	394	73	0,19	70	0,18
LMD5	478	102	0,21	137	0,29
MRI2	374	46	0,12	52	0,14
UGAMP	461	94	0,20	154	0,33
UIUC11	332	31	0,09	40	0,12
UKMO	424	70	0,17	97	0,23
YONU	419	37	0,09	35	0,08
Average	430	70	0,16	93	0,21

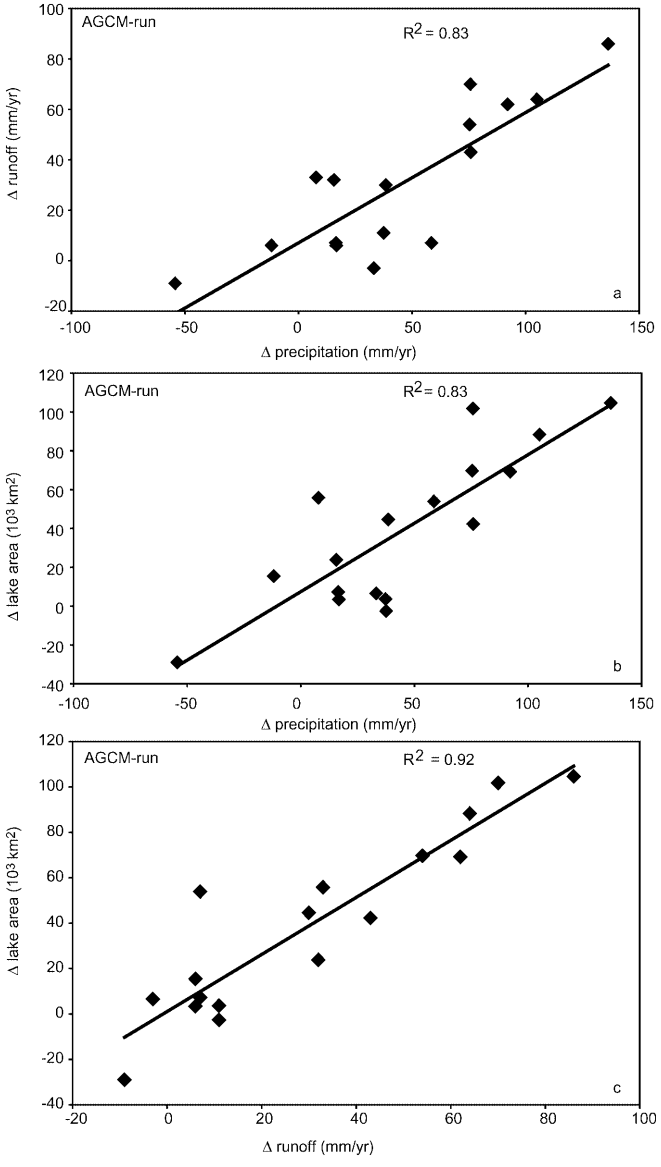

Fig. 3. Correlations between the changes (6 ka–0 ka) in **a** precipitation (mm/year) and runoff (mm/year), **b** precipitation (mm/year) and lake area (km^2), and **c** runoff (mm/year) and lake area (km^2), over northern Africa (10–25°N, 20°W–30°E) as simulated in the HYDRA AGCM-run

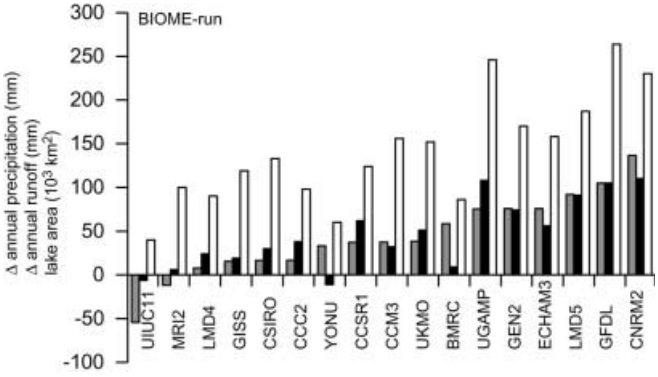

Fig. 4. Changes in annual precipitation (in mm) in *grey* and annual runoff (mm) in *black* simulated by the 17 PMIP models (6 ka BP–0 ka BP) compared to lake area (10^3 km^2) in *white* simulated in the HYDRA BIOME-run, all averaged over northern Africa (10–25°N, 20°W–30°E)

the BIOME-run, which is consistent with the AGCM having much lower runoff and a relatively higher evaporation rate than BIOME3. For example, the largest increase in lake area in BIOME-run compared to AGCM-run occurs for the CCM3, CCSR1, UGAMP, and CSIRO models. BIOME3 simulates an increase in the runoff ratio that is larger than the average for these four models (Table 3). This indicates that for a given energy and water balance the land surface models in these AGCMs have comparatively high evaporation rates; more of the energy is partitioned to evaporation (Table 3, Fig. 7).

The differences between the lake areas for AGCM-run and BIOME-run also help identify those models with energy and water balances that fall outside of the average. For example, the simulated lake area in BIOME-run is less than the AGCM-run only for YONU, LMD4, and BMRC. These three models have very different water balances from one another (Table 3, AGCM runoff ratios from 0.08 to 0.18) but in all three cases the simulate runoff ratio for BIOME-run is not significantly increased compared to AGCM-run (and is in fact decreased in two of the three). As pointed out by Joussaume et al. (1999) these models have a simulated monsoon that is much further north than the other models. Increased runoff at 6 ka BP is simulated by these three models from about 15–25°N and decreased runoff south of 15°N (consistent with a northward shift in the monsoon front). The other models tend to have increased monsoon precipitation and runoff centered further south, at 12–15°N (Fig. 3 of Joussaume et al. 1999). The total lake area in northern Africa is reduced in these three models because; (1) the increased precipitation at 6 ka BP is evaporated from the equilibrium vegetation and land surface (does not form runoff); and (2) decreased precipitation over the Lake Chad basin (south of 20°N) results in less water for runoff and lake formation at that location.

The BIOME-run simulations clearly demonstrate that simulated lake area is affected by the AGCM evaporatranspiration. The differences between the basic model physics in the AGCMs produce very different lake areas. The BIOME-run also points out the importance of the spatial distribution of the precipitation in determining the runoff and lake area. For example, models with nearly identical average precipitation have very different simulated runoff and lake area in BIOME-run (e.g. UGAMP, GEN2, and ECHAM3, Fig. 4, Table 3). The mean potential evaporation calculated from the AGCM simulated temperature and cloudiness differs by less than 2% between the modern and 6 k a simulations for all models (not shown). Therefore, any difference in runoff and lake area in BIOME-run for identical mean precipitation forcing must be a result of

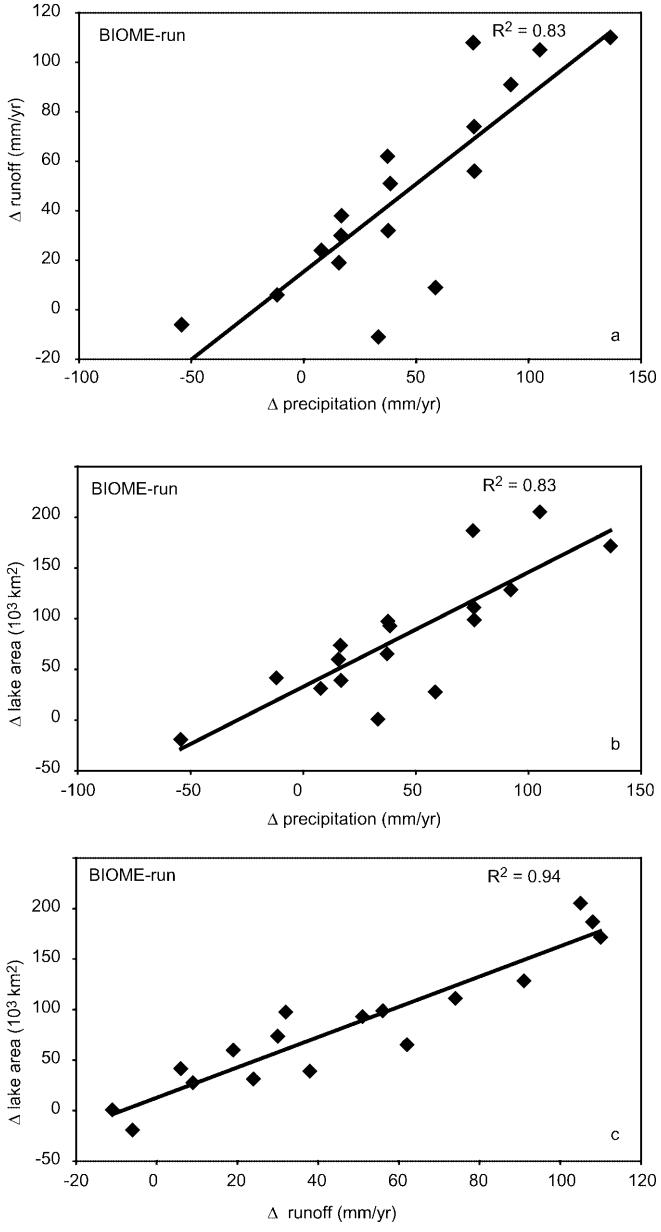

Fig. 5. Correlations between the changes (6 ka–0 ka) in **a** precipitation (mm/year) and runoff (mm/year), **b** precipitation (mm/year) and lake area (km^2), and **c** runoff (mm/year) and lake area (km^2), over northern Africa (10–25°N, 20°W–30°E) as simulated in the HYDRA BIOME-run

differences in where the individual models place the precipitation. Because the pattern of precipitation differs between models the total simulated evapotranspiration differs due to the requirements of the underlying land surface in BIOME3.

5 Analysis and conclusions

Runoff from 17 of the AGCMs participating in PMIP was used as input to the HYDRA model to simulate

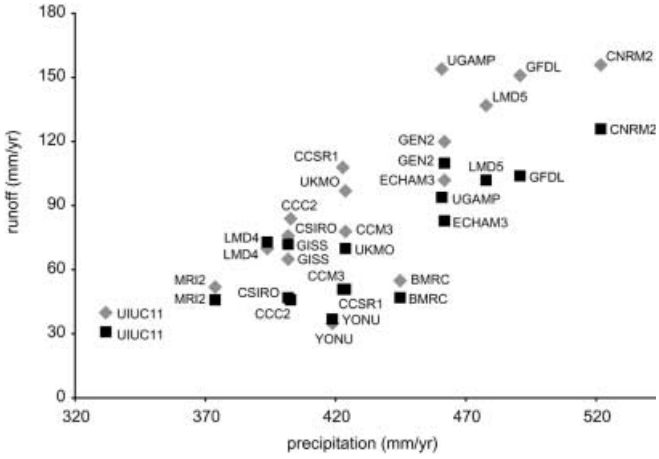

Fig. 6. Correlation between precipitation and runoff over northern Africa generated by each of the PMIP models in AGCM-run (*square symbols*) and BIOME-run (*diamonds*) respectively

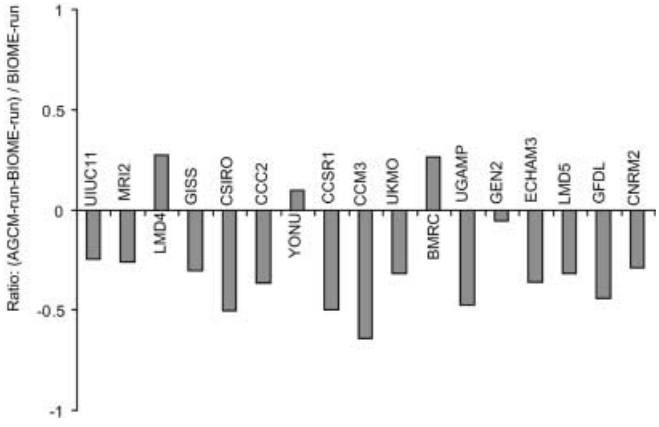

Fig. 7. Comparison of the simulated lake area over northern Africa (10–25°N, 20°W–30°E) from the AGCM-run and BIOME-run, standardized with respect to the BIOME-run results

lake area in northern Africa at 6 ka BP. The AGCMs show a wide range of climatic response to the orbital forcing. The AGCM-simulated runoff produced six-fold differences in simulated lake area between models.

Almost all of the AGCMs produce an expansion of the lake area in northern Africa, consistent with increased monsoon precipitation and hence increased runoff. However, none of the AGCMs produce a sufficient increase in precipitation and runoff to maintain the area of lakes shown by observations. The largest lake area simulated is about 160,000 km^2, which is much less than the 570,000 km^2 observed at 6 ka BP. This result is consistent with previous PMIP analyses, performed by Joussaume et al. (1999) and Harrison et al. (1999), which showed that the simulated precipitation was much less than observations would suggest. In addition, most models tend to overestimate the fraction of lake area in northern Africa associated with the Lake Chad basin compared to the observations of Hoelzmann et al.

(1998). This suggests that there is a tendency by the AGCMs to concentrate the precipitation changes in east-central Africa rather than throughout northern Africa.

There is considerable variation in the magnitude and distribution of the simulated 6 ka BP precipitation changes between the models, which result in large differences in lake area. The wide range in the 6 ka BP simulated lake area in AGCM-run appears to reflect both variations in the magnitude of the simulated precipitation changes, and differences in the simulated runoff due to differences in the land surface models and their parametrizations. However, there is also considerable variation in simulated runoff in AGCM-run, and therefore lake area, that is related to the land surface characterization. For similar changes in precipitation magnitude there is considerable difference in the simulated runoff and lake area (Fig. 1). These differences in simulated runoff are a direct result of differences in where the precipitation changes take place and how the AGCM land surface models redistribute incoming precipitation and energy into latent (evaporation) and sensible heat fluxes and the resultant surface temperature. This result is consistent with the PILPS investigation of surface energy fluxes in land surface models of differing complexity (Desborough 1999).

In our BIOME-run simulations we tested the dissimilarity of the AGCM land surface model simulations. Models for which there is a large difference in simulated lake area (AGCM-run minus BIOME-run) indicate land surface models well outside the mean (e.g. LMD4, YONU, BMRC, CCM3). Desborough (1999) showed that land surface model complexity, by itself, does not guarantee a better simulation of the surface hydrologic balance. Our analyses are consistent with this conclusion. For example, two of the models for which the lake area simulations differ most from the suite of simulations include the least complex (LMD4, bucket model) and most complex (CCM3, LSM) land surface models.

The BIOME-run simulations demonstrate that while runoff is the most important control on simulated lake area ($R^2 = 0.94$), inter-model differences in evaporation (as measured by potential evaporation) exert a significant influence on the simulated lake area. The BIOME-run simulations suggest that the spatial distribution of precipitation, which is related to fundamental differences in model architecture (de Noblet-Ducoudré et al. 2000), may also be important in determining the strength of the overall response to simulated changes in the hydrological cycle.

The PMIP simulations analyzed here were designed to isolate the atmospheric-response to mid-Holocene changes in orbital forcing, and thus ocean conditions and vegetation cover were prescribed to be the same as in the modern (control) simulations. Ocean feedbacks and vegetation feedbacks are known to significantly enhance orbitally induced changes in the African monsoon (Kutzbach et al. 2001). Thus, it cannot be expected that the simplified design used in the PMIP simulations will fully reproduce observed changes in the hydrological cycle and in the extent of lakes in northern Africa. Nevertheless, comparison of the simulated lake area with observations provides a useful benchmark and enables us to quantify to some extent the impact of inter-model differences in land-surface partitioning of surface energy fluxes, and in the spatial distribution of precipitation, on the hydrological cycle simulated by the PMIP AGCMs. The use of more complex models that incorporate ocean- or land-surface feedbacks may improve the overall match to observed changes in monsoon strength in northern Africa (Hewitt and Mitchell 1998; Otto-Bleisner et al. 1999; Braconnot et al. 2000; Doherty et al. 2000), but it is likely that inter-model differences will be as or even more significant than amongst atmosphere-only models. By facilitating quantitative comparisons against benchmark data sets, forward models like HYDRA and BIOME should be a useful component of the diagnostic toolkit used in to evaluate these more complex models.

Acknowledgements We thank Kerstin Sickel for assistance in running the BIOME and HYDRA simulations, Silvana Schott for producing the images, and Pascale Braconnot and Nathalie de Noblet-Ducoudré for discussing the results and suggesting multiple lines for further investigation. We also thank two anonymous reviewers for suggesting numerous improvements to this manuscript. This work is a contribution to the TEMPO (Testing Earthsystem Models with Palaeoenvironmental Observations) project and to PMIP (Palaeoclimate Modelling Intercomparison Project).

References

Arnold M, Petit-Maire N (ed) (1991) Paléoenvironments du Sahara. Lacs holocènes de Taoudenni (Mali). Cent Natl De la Rech Sci, Paris, 237 pp

Berger AL (1978) Long-term variations of caloric solar insolation resulting from the earth's orbital elements. Quat Res 9: 139–167

Bonan GB (1996) A land surface model (LSM version 1.0) for ecological, hydrological, and atmospheric studies: Technical description and user's guide. NCAR Tech. Note NCAR/TN-417-STR, NCAR, Boulder, CO, 165 pp. (available from National Center for Atmospheric Research, PO Box 3000, Boulder, CO 80307)

Bonfils, C, de Noblet-DucoudréN, Braconnot P, Joussaume S (2001) Hot desert albedo and climate change: mid-Holocene monsoon in North Africa. J Clim 14: 3724–3737

Braconnot P, Joussaume S, de Noblet N, Ramstein G, PMIP Participating Groups (2000) Mid-Holocene and last glacial maximum African monsoon changes as simulated within the Paleoclimate Modeling Intercomparison Project. Global Planet Change 26: 51–66

Braconnot P, Marti O, Joussaume S, Leclainche Y (2000) Ocean feedback in response to 6 kyr BP insolation. J Clim 13: 1537–1553

Broström A, Coe M, Harrison SP, Gallimore R, Kutzbach JE, Foley J, Prentice IC, Behling P (1998) Land surface feedbacks and paleomonsoons in northern Africa. Geophys Res Lett 25: 3615–3618

Coe MT, Foley JA (2001) Human and natural impacts on the water resources of the Lake Chad basin. J Geophys Res (Atmos) 106(D4): 3349–3356

Coe MT (1997) Simulating continental surface waters: an application to Holocene Northern Africa. J Clim 10: 1680–1689

Coe MT (1998) A linked global model of terrestrial hydrologic processes: simulation of modern rivers, lakes, and wetlands. J Geophys Res 103: 8885–8899

Coe MT (2000) Modeling terrestrial hydrological systems at the continental scale: testing the accuracy of an atmospheric GCM. J Clim 13: 686–704

Cogley JG (1989) Runoff from the world's landmasses: amounts and uncertainties at 2-degree resolution. Trent Climate Note 89-3, 25 pp (Available from the Department of Geography, Trent University, Peterborough, ON K9J 7B8, Canada)

de Noblet-DucoudréN, Claussen R, Prentice C (2000) Mid-Holocene greening of the Sahara: first results of the GAIM 6000 year BP Experiment with two asynchronously coupled atmosphere/biome models. Clim Dyn 16: 643–659

Desborough CE (1999) Surface energy balance complexity in GCM land surface models. Clim Dyn 15: 389–403

Doherty R, Kutzbach JE, Foley J, Pollard D (2000) Fully-coupled climate/dynamical vegetation model simulations over northern Africa during the mid-Holocene. Clim Dyn 16: 561–573

Dong BW, Valdes PJ (1995) Sensitivity studies of Northern Hemisphere glaciation using an atmospheric general-circulation model. J Clim 8: 2471–2496

Ducoudré N, Laval K, Perrier A (1993) SECHIBA, a new set of parametrizations of the hydrologic exchange at the land–atmosphere interface within the LMD atmospheric general circulation model. J Clim 6: 248–273

Gasse F (1987) Diatoms for reconstructing paleoenvironments and paleohydrology in tropical semi arid zones – example of some lakes from Niger since 12,000 BP. Hydrobiologia 154: 127–163

Ghan SJ, Lingaas JW, Schlesinger ME, Mobley RL, Gates WL (1982) A documentation of the OSU two-level atmospheric general circulation model. Climatic Research Institute, Report 35, Oregon State University: Corvallis, OR, USA, pp 395

Grassl H (2000) Status and improvements of coupled general circulation models. Science 288(5473): 1991–1997

Hall NMJ, Valdes PJ (1997) A GCM simulation of the climate 6000 years ago J Clim 10: 3–17

Harrison SP (2000) Final Report on the Contribution of the Dynamic Palaeoclimatology group at Lund University to the "Evaluating Climate Models with Proxy-Data within the Palaeoclimate Modelling Intercomparison Project". In: Braconnot P (ed) Paleoclimate Modelling Intercomparison Project (PMIP). Proc Third PMIP Workshop, Canada, 4–8 October 1999 WCRP-111, WMO/TD 1007, pp 271

Harrison SP, Jolly D, Laarif F, Abe-Ouchi A, Dong B, Herterich K, Hewitt C, Joussaume S, Kutzbach JE, Mitchell J, de Noblet N, Valdes P (1998) Intercomparison of simulated global vegetation distribution in response to 6 kyr BP orbital forcing. J Clim 11: 2721–2742

Harzallah A, Sadourny R (1995) Internal versus SST-forced atmospheric variability as simulated by an atmospheric general-circulation model. J Clim 8: 474–495

Haxeltine A, Prentice IC (1996) BIOME3: an equilibrium terrestrial biosphere model based on ecophysiological constraints, resource availability and competition among plant functional types. Glob Biogeochem Cycles 10: 693–709

Henderson-Sellers A (1996) Soil moisture simulation: achievements of the RICE and PILPS intercomparison workshop and future directions. Glob Planet Change 13: 99–115

Henderson-Sellers A, Howe W, McGuffie K (1995a) The MECCA analysis project. Glob Planet Change 10: 3–21

Henderson-Sellers A, Pitman AJ, Love PK, Irannejad P, Chen TH (1995b) The Project for Intercomparison of Land-Surface Parametrization Schemes (PILPS): phase 2 and phase 3. Bull Am Meteorol Soc 76: 489–503

Hewitt CD, Mitchell JFB (1997) Radiative forcing and response of a GCM to ice age boundary conditions: cloud feedback and climate sensitivity. Clim Dyn 13(11): 821–834

Hewitt CD, Mitchell JFB (1998) A fully coupled GCM simulation of the climate of the mid-Holocene. Geophys Res Lett 25: 361–364

Hoelzmann P, Jolly D, Harrison SP, Laarif F, Bonnefille R, Pachur H-J (1998) Mid-Holocene land-surface conditions in northern Africa and the Arabian peninsula: a data set for the analysis of biogeophysical feedbacks in the climate system. Glob Biogechem Cycles 12: 35–51

Jolly D, Harrison SP, Damnati B, Bonnefille R (1998) Simulated climate and biomes of Africa during the Late Quaternary: comparison with pollen and lake status data. Quat Sci Rev 17: 629–657

Joussaume S, Taylor KE (1995) Status of the Paleoclimate Modeling Intercomparison Project (PMIP). In: Gates WL (ed) "Proc First International AMIP Sci Conf, 15–19 May 1995." CRP-92 WMO/TD 732, Monterey, CA, USA, pp 532

Joussaume S, Taylor KE (2000) The Paleoclimate Modeling Intercomparison Project. In: Braconnot P (ed) Paleoclimate Modelling Intercomparison Project (PMIP). Proc Third PMIP Workshop, Canada, 4–8 October 1999. WCRP-111, WMO/TD 1007

Joussaume S, Taylor KE, Braconnot P, Mitchell JFB, Kutzbach J, Harrison SP, Prentice IC, Broccoli AJ, Abe-Ouchi A, Bartlein PJ, Bonfils C, Dong B, Guiot J, Herterich K, Hewitt CD, Jolly D, Kim JW, Kislov A, Kitoh A, Loutre MF, Masson V, McAvaney B, McFarlane N, de Noblet N, Peltier WR, Peterschmitt JY, Pollard D, Rind D, Royer JF, Schlesinger ME, Syktus J, Thompson S, Valdes P, Vettoretti G, Webb RS, Wyputta U (1999) Monsoon changes for 6000 years ago: results of 18 simulations from the Paleoclimate Modeling Intercomparison Project (PMIP). Geophys Res Lett 26: 859–862

Kattenberg A, Giorgi F, Grassl H, Meehl GA, Mitchell JFB, Stouffer RJ, Tokioka T, Weaver AJ, and Wigley TML (1996) Climate models projections of future climate. In: Houghton JT, Meira Filho LG, Callander BA, Harris N, Kattenberg A, Maskell K. (eds). Climate change 1995: the science of climate change. Cambridge University Press, Cambridge, United Kingdom, pp 285–357

Kiehl JT, Boville B, Briegleb B, Hack J, Rasch P, Williamson D (1996) Description of the NCAR Community Climate Model (CCM3). NCAR Tech Note NCAR/TN-420+STR, NCAR, Boulder CO (available from National Center for Atmospheric Research, PO Box 3000, Boulder, CO 80307), pp 152

Kitoh A, Noda A, Nikaidou Y, Ose T, Tokioka T (1995) AMIP simulations of the MRI GCM. Pap Meteorol Geophys 45: 121–148

Kitoh A, Yamazaki K, Tokioka T (1998) Influence of soil moisture and surface albedo changes over the African tropical rain forest on summer climate investigated with the MRI GCM-I. J Meteorol Soc Japan 66: 65–86

Kohfeld KE, Harrison SP (2000) How well can we simulate past climates? Evaluating the models using global palaeoenvironmental datasets. Quat Sci Rev 19: 321–346

Kowalczyk EA, Garratt JR, Krummel PB (1994) Implementation of a soil-canopy scheme into the CSIRO GCMs, CSIRO Division of Atmospheric Research, Technical Paper, 32

Kowalczyk EA, Garratt JR, Krummel PB (1991) A soil-canopy scheme for use in a numerical model of the atmosphere-1D Stand-Alone Model, CSIRO Division of Atmospheric Research, Technical Paper 23

Kutzbach JE, Harrison SP, Coe MT (2001) Land-ocean-atmosphere interactions and monsoon climate change: a palaeoperspective. In: Schulze E-D, Heimann M, Harrison SP, Holland E, Lloyd J, Prentice IC, Schimel D (eds) Global biogeochemical cycles in the climate system. Academic Press, New York, pp 73–86

Leemans R, Cramer W (1991) The IIASA climate database for mean monthly values of temperature, precipitation and cloudiness on a global terrestrial grid. RR-91–18, International Institute for Applied Systems Analysis, Laxenburg, Austria

Legates DR, Willmott CJ (1990a) Mean seasonal and spatial variability in gauge-corrected, global precipitation. Int J Climatol 10(2): 111–127

Legates DR, Willmott CJ (1990b) Mean seasonal and spatial variability in global surface air-temperature. Theor Appl Climatol 41(1–2): 11–21

Lenters JD, Coe MT, Foley JA (2000) Surface water balance of the continental United States, 1963–1995: regional evaluation of a terrestrial biosphere model and the NCEP/NCAR reanalysis. J Geophys Res (Atmos) 105: 22, 393–22, 425

Lorenz S, Grieger B, Helbig P, Herterich K (1996) Investigating the sensitivity of the atmospheric general circulation model ECHAM 3 to paleoclimatic boundary conditions. Geol Rundsch 85: 513–524

Mahfouf JF, Manzi AO, Noilhan J, Giordani H, Deque M (1995) The land-surface scheme ISBA within the meteo-France climate model ARPEGE. 1. Implementation and preliminary-results. J Clim 8(8): 2039–2057

Maley J (1981) Etudes palynologiques dans le bassin du Tchad et paléoclimatologie de l'Afrique nord-tropicale de 30,000 ans àl'époque actuelle. Tech rep 129, Inst. Fr. de Rech. Sci. pour le Dev. en Cooperation (ORSTOM), Paris, France

Maley J (1983) Histoire de la végétation et du climat de l'Afrique nord-tropicale au Quaternaire récent. Bothalia 14: 377–389

Manabe S (1969) Climate and the ocean circulation. I. The atmospheric circulation and the hydrology of the earth's surface. Mon Weather Rev 97: 739–774

Manabe S, Smagorinsky J, Strickler RF (1965) Simulated climatology of a general circulation model with a hydrologic cycle. Mon Weather Rev 93: 769–798

Mann ME, Park J, Bradley RS (1995) Global interdecadel and century-scale climate oscillations during the past five centuries. Nature 378: 266–270

Manzi AO, Planton S (1994) Implementation of the ISBA parametrization scheme for land-surface processes in a GCM: an annual cycle experiment. J Hydrol 155(3–4): 353–387

Masson V, Joussaume S (1997) Energetics of the 6000-year BP atmospheric circulation in boreal summer, from large-scale to monsoon areas: a study with two versions of the LMD AGCM. J Clim 10(11): 2888–2903

McAvaney BJ, Hess GD (1996) The revised surface fluxes parametrization in the BMRC AGCM: formulation. BMRC Research Rep 56, Bureau of Meteorology Research Centre, Melbourne, Australia

McFarlane NA, Boer GJ, Blanchet J-P, Lazare M (1992) The Canadian Climate Centre second-generation general circulation model and its equilibrium climate, J Clim 5: 1013–1044

Miller MJ, Beljaars ACM, Palmer TN (1992) The sensitivity of the ECMWF model to the parametrization of evaporation from the tropical oceans. J Clim 5: 418–434

Monteith JL (1995) Accommodation between transpiring vegetation and the convective boundary layer. J Hydrol 166: 251–263

Moore III B, Cramer W, Rasool I, Sahagian D, Steffen W, Participants in "POTSDAM 95" (1995) Global net primary productivity: report of the Potsdam '95 IGBP NPP Model Intercomparison Workshop (GAIM-DIS-GCTE) Potsdam, Germany, June 20-22, 1995. Abstracts, GAIM First Sci Conf, 25–29th September 1995, Garmisch-Partenkirchen, Germany

Noda A, Tokioka T, Nikaidou Y, Nakagawa S, Takata K (1995) Improvement of a cryospheric model for climate modeling. Proc Int Arctic Symp, Tsukuba, January 12–13, 1995, A34–A40, Science and Technology Agency, and Japan Marine science and Technology Center

Noilhan J, Planton S (1989) A Simple parametrization of land surface processes for meteorological models. Mon Weather Rev 117(3): 536–549

Otto-Bliesner BL (1999) El Niño, La Niña and Sahel precipitation during the middle Holocene. Geophys Res Lett 26: 87–90

Pachur H-J, Hoelzmann P (1991) Paleoclimatic implications of late Quaternary lacustrine sediments in western Nubia, Sudan. Quat Res 36: 257–276

Pachur H-J, Kröpelin S (1987) Wadi Howar: Paleoclimatic evidence from an extinct river system in the Southeastern Sahara. Science 237: 298–300

Peixóto JP, Oort AH (1992) Physics of climate. American Institute of Physics, 520 pp

Petit-Maire N (1989) Interglacial environments in presently hyperarid Sahara: Palaeoclimatic implications, in: Leinen N, Sarnthein M (Eds) Paleoclimatology and paleometeorology: modern and past patterns of global atmosphereric transport, Kluwer Acad., Norwell, Mass, pp 637-661

Petit-Maire N, Riser J (1981) Holocene lake deposits and palaeoenvironments in central Sahara, Northeastern Mali. Palaeogeogr Palaeoclimatol Palaeoecol 35: 45–61

Petit-Maire N, Riser J (1983) Sahara ou Sahèl? Quaternaire récent du Bassin de Taoudenni (Mali), Cent Natl De la Rech. Sci, Paris, 473 pp

Pias J (1970) Les formation sédimentaires tertiaires et quaternaires de la cuvette tchadienne et les sols qui en derivent. Mémoires, ORSTOM 43: 1–408

Pitman AJ, Henderson-Sellers A, Abramopoulos F, Avissar R, Bonan G, Boone A, Cogley JG, Dickinson RE, Ek M, Entekhabi D, Famiglietti J, Garratt JR, Frech M, Hahmann A, Koster R, Kowalczyk E, Laval K, Lean L, Lee TJ, Lettenmaier D, Liang X, Mahfouf J-F, Mahrt L, Milly C, Mitchell K, de Noblet N, Noilhan J, Pan H, Pielke R, Robock A, Rosenzweig C, Running SW, Schlosser A, Scott R, Suarez M, Thompson S, Verseghy D, Wetzel P, Wood E, Xue Y, Yang Z-L, Zhang L (1993) Results from the off-line control simulation phase of the Project for Intercomparison of Land surface Parametrisation Schemes (PILPS), GEWEX Tech Note, IGPO Publ Ser 7, pp 47

Pollard D, Thompson SL (1995) Use of a land-surface-transfer scheme (LSX) in a global climate model: the response to doubling stomatal resistance. Global Planet Change 10: 129–161

Pollard D, Bergengren JC, Stillwell-Soller LM, Felzer B, Thompson SL (1998) Climate simulations for 10,000 and 6000 years BP using the GENESIS global climate model. Paleoclim - Data Model 2: 183–218

Qin B, Harrison SP, Kutzbach JE (1998) Evaluation of modelled regional water balance using lake status data: a comparison of 6ka simulations with the NCAR CCM. Quat Sci Rev 17: 535–548

Raynaud D, Jouzel J, Barnola JM, Chappellaz J, Delmas RJ, Lorius C (1993) The ice record of greenhouse gases. Science 259: 926–934

Ritchie JC, Haynes CV (1987) Holocene vegetation zonation in the eastern Sahara, Nature 330: 645–647

Ritchie JC, Eyles CH, Haynes CV (1985) Sediment and pollen evidence for an early to mid-Holocene humid period in the eastern Sahara. Nature 314: 352–355

Rosenzweig C, Abramopoulos F (1997) Land-surface model development for the GISS GCM. J Clim 10(8): 2040–2054

Rowell DP, Folland CK, Maskell K, Ward MN (1995) Variability of summer rainfall over tropical North Africa (1906–92): observations and modelling. Quat J R Meteorol Soc 121: 669–704

Sadourny R, Laval K (1984) January and July performance of the LMD general circulation model. In: Berger AL, Nicolls C (eds) New perspectives in climate modelling. Elsevier, Paris, pp 173–197

Schneider JL (1967) Evolution du dernier lacustre et peuplements préhistoriques aux Bas-Pays du Tchad, bulletin, Associations Sénégalaise pour l'Etude du Quaternaire en Afrique, Sénégale, pp 18–23

Schulz E (1991) The Taoudenni-Agorgott pollen record and the Holocene vegetation history of the Central Sahara, In: (ed) Petit-Maire N. Paléoenvironnements du Sahara. Lacs holocènes àTaoudenni (Mali) Cent. Natl. De la Recherch Sci, Paris, pp 143–162

Shao Y, Anne RD, Henderson-Sellers A, Irannejad P, Thornton P, Liang X, Chen TH, Ciret C, Desborough C, Balachova O, Haxeltine A, Ducharne A (1994) Soil moisture simulation a Report of the RICE and PILPS Workshop. International GEWEX Project Office, Report, 14, pp 1789

Street FA, Grove AT (1976) Environmental and climatic implications of late Quaternary lake-level fluctuations in Africa. Nature 261: 385–390

Street-Perrott FA, Perrott RA (1993) Holocene vegetation, lake levels, and climate of Africa. In Wright Jr HE, Kutzbach JE, Webb III T, Ruddiman WF, Street-Perrott FA, Bartlein PJ (eds). Global Climates since the Last Glacial Maximum. University of Minnesota Press, Minneapolis, pp 318–356

Tett SFB, Stott PA, Allen MR, Ingram WJ, Mitchell JFB (1999) Causes of twentieth-century temperature change near the Earth's surface. Nature 399(6736): 569–572

Texier D, de Noblet N, Harrison SP, Haxeltine A, Jolly D, Joussaume S, Laarif F, Prentice IC, Tarasov PE (1997) Quantifying the role of biosphere-atmosphere feedbacks in climate change: coupled model simulation for 6000 years BP and comparison with palaeodata for northern Eurasia and northern Africa. Clim Dyn 13: 865–882

Tokioka T, Yamazaki K, Yagai I, Kitoh A (1984) A description of the Meteorological Research Institute atmospheric general circulation model (MRIGCM-I). MRI Tech Rep 13, Meteorological Research Institute, Ibaraki-ken, Japan, pp 249

Valdes P, Hall NMJ (1994) Mid-latitude depressions during the ice age. In: Duplessy J-C, Spyridakis M-T (eds) Long term climatic variations: data and modelling. Springer Berlin Heidelberg, New York, pp 511–531

Vettoretti G, Peltier WR, McFarlane NA (1998) Simulations of mid-Holocene climate using an atmospheric general circulation model. J Clim 11: 2607–2627

Warrilow DA, Sangster AB, Slingo A (1986) Modelling of land surface processes and their influence on European climate. Techn rep DCTN 38, Dynamical Climatology Branch, United Kingdom Meteorological Office, Bracknell, Berkshire RG12 2SZ, UK, pp 92

Warrilow DA, Buckley E (1989) The impact of land surface processes on the moisture budget of a climate model. Ann Geophys 7: 439–450

Wilson MF, Henderson-Sellers A (1985) A global archive of land cover and soils data for use in general circulation climate models. J Clim 5: 119–143

Yu G, Harrison SP (1996) An evaluation of the simulated water balance of Eurasia and northern Africa at 6000 years BP using lake status data. Clim Dyn 12: 723–735